JOURNAL OF Applied Polymer SCIENCE

Pattern Formation and Morphology in the Course of Drying a Droplet of a Ternary Polymer Solution

Xiaoli Sun,[1,2] Huihui Li,[1] Shouke Yan,[1] Ingo Lieberwirth[2]

[1]State Key Laboratory of Chemical Resource Engineering, Beijing University of Chemical Technology, Beijing 100029, China

[2]Max Planck Institute for Polymer Research, Mainz, Germany

Correspondence to: S. Yan (E-mail: skyan@mail.buct.edu.cn)

ABSTRACT: A micro-structured polymer film was prepared by drying a droplet of a ternary polymer solution of polystyrene (PS), poly(vinyl pyrrolidone) (PVP), and chloroform. Within a certain weight ratio of PS to PVP an ordered pattern of cylindrical PVP domains was formed on the film surface. The diameter of the individual PVP domains was in the order of 2–3 μm. The effect of polymer weight ratios on the surface morphology was investigated by atomic force microscopy. Additionally, scanning electron microscopy of cross-sections of the polymer composite film yielded supplementary information on the bulk morphology and revealed an unexpected complex structure underneath the surface pattern. The reasons for this formation mechanism possibly included aspects of phase separation, convective transport in a drying droplet, and the continuous increase of viscosity during solvent evaporation. At a certain solvent concentration in the evaporation path, it will lead to a vitrification of any structure. The "evolution time", the time between the onset of phase separation and this "point of vitrification", will determine the resulting film morphology. © 2012 Wiley Periodicals, Inc. J. Appl. Polym. Sci. 129: 1784–1792, 2013

KEYWORDS: blends; phase behavior; films

Received 16 August 2012; accepted 24 November 2012; published online 22 December 2012

DOI: 10.1002/app.38876

INTRODUCTION

In recent years, interest in microporous polymer films has steadily increased due to the potential applications in photonics, opto-electronic devices, catalysis, and membranes.[1–3] The microporous polymer films can be prepared by using synthesized polymer or physical method. Both methods are widely used into different fields. Usually there are two physical methods. One method is the templating approach which uses colloidal crystals,[4] microphase-separation of block copolymers,[5] and polymers with a rod-coil structure.[6] Another frequently used method is phase separation processes. Various morphologies can be achieved in this way. Generally, this method is based on the thermodynamically driven phase separation of two immiscible materials from a common solvent, either by means of temperature control or solvent evaporation. Solvent evaporation is an elegant way of preparing thin microstructured films by controlling the major process of relevant parameters including solvent evaporation rate, thickness of the initial liquid layer, and composition of the polymer blend solution. For instance, various interface morphologies controlled by the interplay of phase separation and dewetting were prepared by spincoating polymer blend solutions with different compositions.[7] Han et al. developed a simple route for fabricating 2D and 3D micropatterned polymer films by spreading a polymer solution on the surface of a nonsolvent or coating a stable polymer–solvent–nonsolvent solution on a solid substrate surface.[8,9] By adjusting the evaporation rate and the polymer components ratio, symmetrical patterns in a polystyrene/poly(2-vinylpyridine) system could be obtained.[10] Apart from the phase separation, the understanding of the formation of self assembled, regular structures requires involvement of an additional effect that is periodic in lateral direction. Development of Bènard–Marangoni instabilities is one possible way to achieve a periodic disturbance of the fluid surface.[11] In a drying fluid film with a horizontal air-liquid interface Marangoni convection can occur under certain conditions, resulting in a two-dimensional, wavelike surface. Evaporation of the solvent on the air-liquid interface consumes latent heat and thus creates a temperature gradient from bottom to top. Statistical fluctuations in the local temperature are likely to occur at the liquid-air interface and eventually create some transient "hot spots". The transient "hot spot" on the surface reduces the local surface tension at the liquid-air interface. Consequently, a valley will be formed at the place of "hot spot". With the temperature increasing, the "valley" approaches the substrate, moreover the surface tension decreases further. Hence,

Additional Supporting Information may be found in the online version of this article.

this instability is enhanced and spreads laterally. The difference in surface tension is the driving force for this kind of convection. The dimensionless Marangoni-number

$$\mathrm{Ma} = [-(d\gamma/dT)\Delta Th]/\rho\nu\kappa$$

gives an indication of the occurrence of Bènard–Marangoni convection. It describes the competition between the driving force $d\gamma/d$T (γ: surface tension of the fluid) and the action of ρ, ν, and κ being the density, the kinematical viscosity and the thermal diffusivity of the fluid layer, respectively. ΔT denominates the temperature gradient over the height h of the fluid layer. Typically, Marangoni convection leads to the formation of regular, hexagonally arranged convective cells with a characteristic scale in the order of 1–3 times the height of the liquid film.[11,12] The transition from disordered structure to ordered patterns occurs for Ma $>$ 80.[13] Kumacheva et al. carefully examined the formation of regular patterns emerging from drying a polystyrene–polymethylmethacrylate blend solution in toluene.[14,15] By controlling the initial film thickness and the evaporation rate of the solvent, they could tune the Marangoni number of the system up to 500 and found that ordered patterns form for systems with Ma $>$ 90.

For ternary blend systems containing polystyrene (PS) and poly(2-vinylpyridine) similar surface patterns can be found after drying a thin film and Marangoni instability is claimed to be responsible for this microstructure patterning.[10,16–18] However, calculation of Ma in a ternary system that constantly changes its composition, the viscosity, density, and thermal diffusivity, is not an easy task, especially when liquid–liquid phase separation has to be taken into consideration as well.

Kim et al. observed micro pattern formation when drying a polystyrene/polyethyleneglycol blend, but did not find any influence of the initial film thickness on the occurrence of ordered structures. They suggested that capillary instabilities were the driving force behind structure formation.[19] Bormashenko et al. proposed an alternative physical mechanism for the formation of micropatterns in binary polymer solutions.[20] Based on the concentration gradient over the film thickness, a convective flow emerges that is stabilized and amplified by the surface tension difference between the solvent-rich and the solvent-poor surface areas.[21]

Obviously, the processes occurring in a drying droplet of a ternary polymer solution of immiscible polymers are fairly complex and interdependent. And accordingly this might be the reason for the discrepancies on the origin of the ordered pattern formation found in literature. However, it can not be totally excluded that different polymer/solvent combinations will generate similar ordered surface patterns resulting from very different physical processes. Yet another aspect that might help purging this formation process is the inspection of the bulk structure of the resulting film. This has widely been neglected so far although it can supply helpful information for retracing the formation process of the surface pattern. In our recent work, we chose PS and poly(vinyl pyrrolidone) (PVP) as immiscible polymer system and dissolved them in chloroform, which is a common solvent for these polymers. The morphological evolution with different PS/PVP weight ratio was investigated and discussed carefully. In addition to the conventional surface characterization, a cross section of the resulting film was investigated by scanning electron microscopy (SEM). Based on these findings, we propose a simple formation mechanism for the observed surface pattern. It is based on the interplay of the liquid–liquid phase separation and the increase of viscosity due to evaporation of the solvent.

EXPERIMENTAL

PS with an average molecular weight of 280,000 g/mol and PVP with an average molecular weight of 44,000 g/mol were purchased from Aldrich Chemical Company. They were dissolved in chloroform (0.9wt %) with weight ratios of PS/PVP changing from 10/90 to 90/10. The polymer solutions were filtered with a 0.22 μm Millipore membrane and then cast onto a microscope slide positioned in the base part of a Petri dish. By using a micro-injector the volume of each drop of solution was adjusted to 15 μL. Directly after applying the solution onto the microscope slide, the Petri dish was closed in order to achieve stable evaporation rates. The evaporation time is $<$2 minutes.

Atomic force microscopy (AFM) measurements were performed on Digital Instruments Dimension 3100 scanning force microscope in the tapping mode with an Olympus cantilever (spring constant in the range of 33.2–65.7 N/m and resonant frequency of 277.3–346.3 kHz).

SEM examination was conducted on a LEO Gemini 1530; the micrographs were taken at low kV conditions without any surface coating. For cross-section imaging, the samples were broken at liquid nitrogen temperature.

Gel permeation chromatography (GPC) vs. poly(styrene) standard was carried out at 60°C using an SDV (from PSS) column, an ERC RI-7512 differential refractometer (ERMA Inc.) and a UV S-3702 (SOMA) detector, and DMF as the eluent. Prior to chromatography, the samples were filtered through a 0.2-μm Teflon filter (Millipore) to remove insoluble impurities.

For identification of the PS and PVP rich phase in AFM and SEM measurements, a selective solvent treatment of the received films was performed. Cyclohexane is good solvent for PS and poor solvent for PVP. So it is used to selectively dissolve PS. For surface profile, the Dektak profilemeter is employed.

RESULTS

The effects of different weight ratios of PS/PVP on the surface structure after casting from a chloroform solution (0.9wt %) on glass substrate were investigated. After drying at ambient conditions, different morphologies, ranging from irregular to aligned structures, were observed.

For low fractions of PS the resulting surface morphology exhibited irregular sized islands of PS emerging from the PVP matrix, which can be seen in Figure 1 for the weight ratios of 10/90 and 20/80 of PS/PVP, respectively. The chemical nature of the islands was verified by using the selective solvent method. The PS domains protrude from the surface presumably due to the lower density of the PS rich liquid phase which forms upon

Applied Polymer SCIENCE

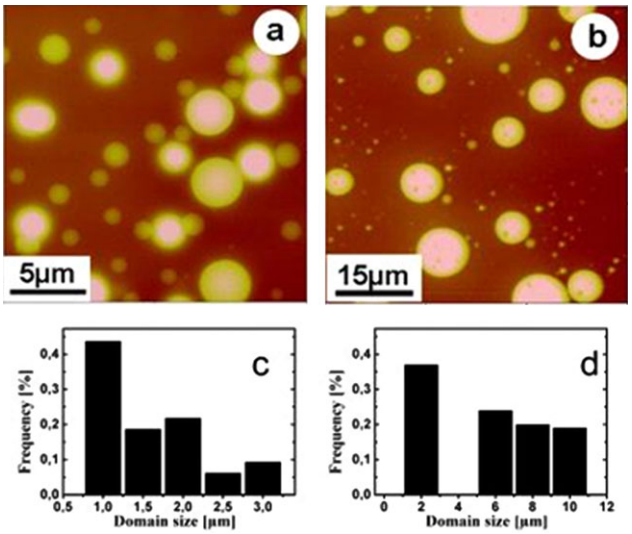

Figure 1. AFM topographical micrographs of a PS/PVP blend cast on a glass substrate from chloroform solution (0.9wt %) with composition ratios of (a) 10/90 and (b) 20/80 and the corresponding size distribution histograms for the PS-rich domains in (c) and (d), respectively. [Color figure can be viewed in the online issue, which is available at wileyonlinelibrary.com.]

phase separation and will float on the surface of the PVP rich liquid phase. For the 10/90 PS/PVP blend the size distribution of the PS islands comprised diameters ranging from 1 to 3.5 μm, whereas for the 20/80 blend the PS islands grew much bigger, reaching diameters up to 11 μm. The corresponding histograms show that the small particles are the major component by frequency. It is interesting to note that for the 20/80 blend the size distribution of the islands shows the absence of medium sized islands (3–5 μm). In systems characterized by a large ratio of major-to-minor components, phase separation is expected to occur in the metastable regime via nucleation and growth, as reported by Cumming et al.[22–25] They observed the formation of spherical, monodisperse droplets of the minority phase by quenching a binary polymer melt into the metastable regime between the binodal and the spinodal curve of the phase diagram. Likewise, the evaporation of the solvent in a binary polymer solution traversed the same area of the phase diagram. Following this process, coalescence will produce larger particles. However, since in our experimental setup we do not apply a sudden quench rather than a slow evaporation, it is reasonable that the phase transition does not occur uniformly over the complete sample and result in an effective induction period for the nucleation and growth of new particles. Accordingly, histograms in Figure 1(c,d) reflect the convolution of the coalescence process and a certain induction period during which new particles were formed continuously. Further increment of the PS fraction to 30% results in a morphology characterized by the coexistence of two different phase morphologies: one is the PS-rich phase and the other is the PVP-rich phase, shown by the optical micrograph in Figure 2. The individual domains of these phases can reach dimensions up to 1 mm in size. However, a reliable identification of the phases observed in the optical micrograph was not possible.

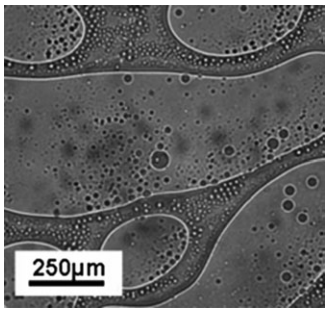

Figure 2. Optical micrograph of a drop dried from a PS/PVP 30/70 blend solution.

This situation of two coexisting phase structures can similarly be found in a composition of 40/60 PS/PVP. However, in this case the different morphologies show up in the centre and at the edge of the dried cast polymer spot, respectively. Figure 3 shows the two kinds of dominant morphologies that can be found at the different positions of the spot. At the edge area one can observe holes emerging from the matrix material and their diameter ranges between 1.5 to 4.8 μm. Fourier analysis of the micrographs from the rim area reveals a poorly ordered closed packed symmetric assembly. In contrast, the central area features a completely different morphology with some irregular distributed elevations. The elevations emerge from the matrix with diameters between 0.7 and 3.6 μm, which is similar to the morphology emerging from the 10/90 PS/PVP blend. This implies that the PS concentration in the central region is significantly depleted in favor of PS accumulation at the rim area of the dried spot. The convective outward transport of the PS is demonstrated in Figure 4(a). Pure solutions of PS and PVP in chloroform have been cast on a glass substrate and the remaining spot is measured by a surface profiler, yielding the local thickness of the polymer film as a function of the distance from the centre of the dried spot. For the PVP solution, the radial thickness of the remaining polymer film was nearly constant, whereas for the PS solution the radial film thickness increased with the distance from the centre. At the very edge of the spot the film thickness increased rapidly forming a kind of a steep wall around the spot. This behavior is known from the coffee-

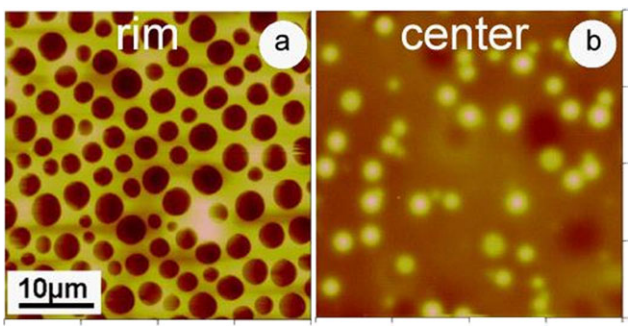

Figure 3. AFM topographical images of PS/PVP blend at a weight ratio of 40/60 showing the different surface morphologies at the rim of the dried droplet (a) and in the central area (b), respectively. [Color figure can be viewed in the online issue, which is available at wileyonlinelibrary.com.]

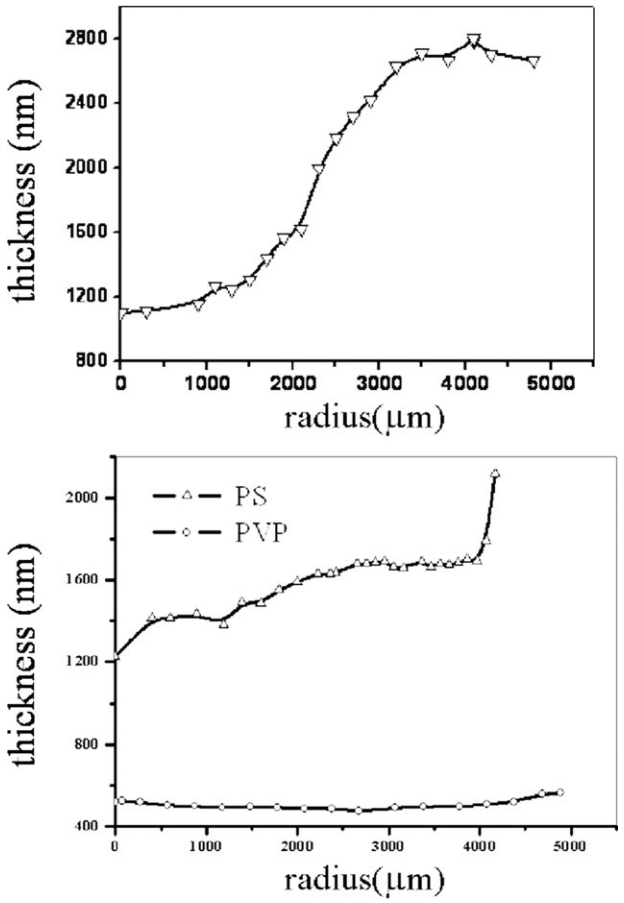

Figure 4. Plots of the thickness vs. the distance from the center of the dried drop. Plot (a) corresponds to the PS/PVP (40/60). Plot (b) corresponds to the pure PS (Δ) and PVP (○) solution.

spot effect[26] and results from the pinning of the contact line of the drying drop in combination with a capillary outward flow of the solvents in the solution. By comparing the radial thickness of neat PS and PVP, it can be seen that PS is much more moveable along the radial direction in the outward flow. For the 40/60 PS/PVP blends the film thickness increased by a factor of 3 from the centre to the edge area [Figure 4(b)]. Although it is evident from the morphological differences between the central and the edge area that the PS is the more mobile component, it is hard to understand why only the PS molecules from the homogeneous ternary solution are subject to the capillary outward flow. However, one has to consider that during the drying process the system undergoes a phase separation, yielding phases differing in viscosity, density, and molecular composition. The mass flow is highest at the liquid/air interface[26] and zero at the bottom of the drop, e.g. the liquid substrate interface. At some point during the evaporation of the solvent, the system will undergo a phase separation forming two phases: one is rich in PS and the other one is rich in PVP. Accordingly, since the PS is found to be enriched in the outward region of the dried spot, phase separated PS rich solution has to be assumed to migrate to the top of the drop (the liquid/air interface), most likely due to its lower density compared to the PVP rich phase.

For PS fractions ranging from 50 to 70% the surface morphology is demonstrated in Figure 5(a,b). Within this compositional range the surface morphology does not change significantly from the centre area to the edge area. Evaporation of the solvent leaves a pattern of aligned holes with an average diameter of 2.1 μm. Fourier analysis of the micrographs does not clearly shows either a hexagonal or a four-fold symmetry [inset in Figure 5(a,b)]. The average length between the holes is 3.2 μm for the 50/50 blend and 3.5 μm for the 70/30 PS/PVP solution. The thermal stability of the polymer films has been examined. By using AFM equipped with hot stage, we find that the morphologies of the films do not change even when the temperature reaches 190°C, suggesting the structures are very stable. Due to the limitation of the instrument, the experiment cannot be carried out at temperature higher than 190°C. The AFM images of 50/50 PS/PVP as an example under thermal treatment can be seen in Figure S1 in Supporting Information.

To characterize the surface composition, the selective solvent etching method was used to identify the composition of the observed surface structure. After selectively dissolving the PS with cyclohexane, the 50/50 PS/PVP blend shows an inverted surface morphology [Figure 5(c)]. Spherical elevations show up in the AFM height image, their diameter and arrangement equals to those observed from the initial structure before selective etching [Figure 5(a)] with a few spots appearing to have been washed away. Accordingly, the initial surface structure can be identified: the elevated matrix consists of PS and the spherical cavities represent the PVP in Figure 5(a). For the 70/30 PS/

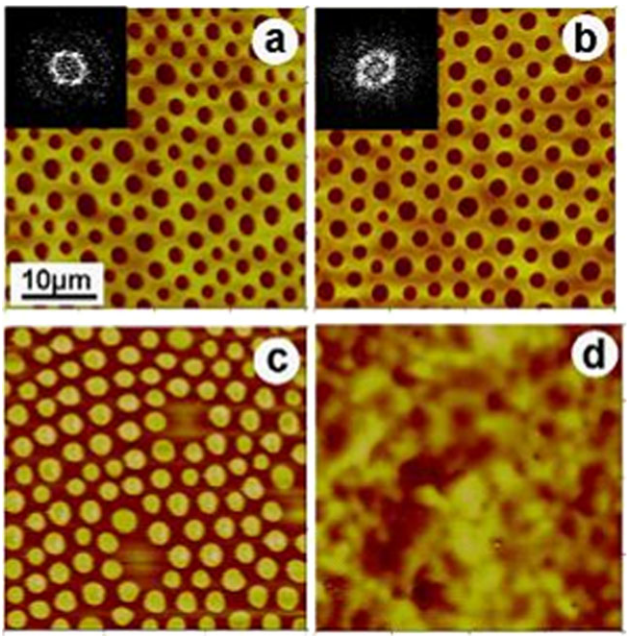

Figure 5. AFM topographical images of PS/PVP blends with weight ratios of 50/50 (a) and 70/30 (b) with the corresponding Fourier transform inserted. After treatment with cyclohexane the surface morphology changed to (c) a nearly inverse structure for the 50/50 PS/PVP composition and (d) to a smooth, unstructured surface for the 70/30 blend, respectively. [Color figure can be viewed in the online issue, which is available at wileyonlinelibrary.com.]

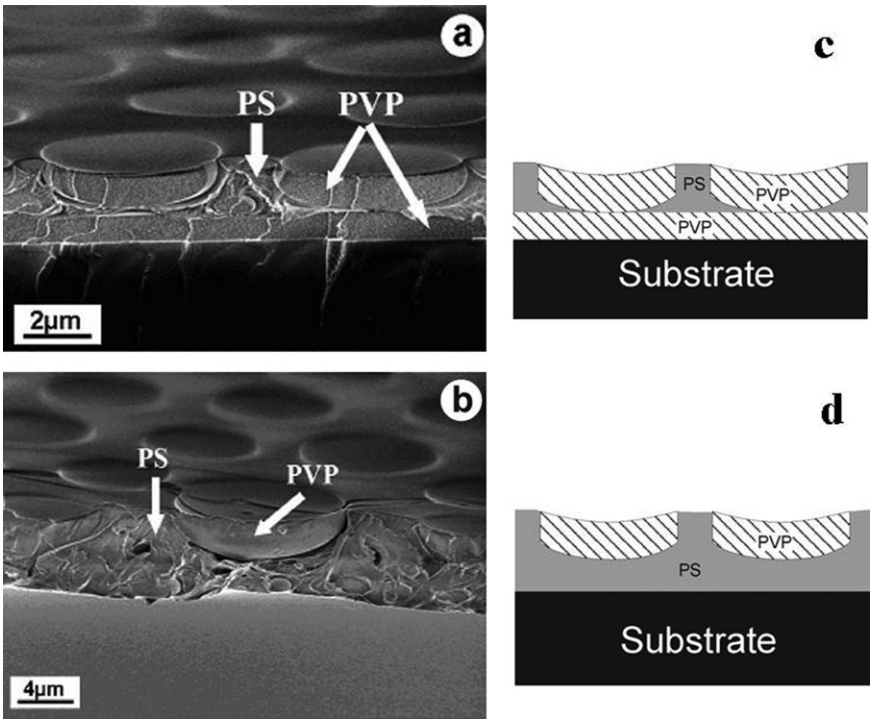

Figure 6. SEM micrographs of the cross section of (a) PS/PVP (50/50) and (b) (70/30) blend with the corresponding compositional sketches on the right hand side, respectively. Identification of the identity of the two observed polymeric phases is based on the selective dissolution experiments.

PVP blend the same selective etching of PS yields a completely different result. The AFM height image [Figure 5(d)] only shows an unstructured, undulated surface remaining on the substrate. When selectively dissolving the PVP of this sample, the entire film is removed from the substrate and drifts on the water surface, indicating that the PS forms a continuous layer. Otherwise the film would have been disintegrated by the water. On the other hand, PVP is supposed to form a continuous layer at the substrate, explaining the easy floating off of the polymer film.

SEM micrographs of the cross-section well illustrate the film morphology (Figure 6). Disc-like PVP droplets are embedded in a PS matrix. For the 50/50 PS/PVP blend the bottom side of these discs contacts a homogeneous PVP layer, which has formed directly on the substrate, as depicted in the sketch of Figure 6(c). An increase of the PS fraction to 70% yields a similar micrograph but an additional layer of PVP could not be identified [Figure 6(b)]. However, electron microscopy can hardly produce a contrast between different polymers. Hence, the existence of a thin layer of PVP on the substrate can not be excluded from the SEM measurement. Taking into account the water dissolution behavior (e.g. floating off the film) one would expect that at least a very thin polymer layer exists on the substrate surface. Because the amount of PS is more than that of PVP, one can expect the thin polymer layer on the substrate is PS layer. Accordingly, Figure 6(d) clarifies the supposed structure of the dried 70/30 PS/PVP blend film.

When increasing the PS fraction further the periodicity disappears. Tiny holes, randomly distributed on the surface are found for 90/10 PS/PVP blends (Figure 7). The diameter of the holes is about 1.2 μm; a uniform arrangement is not obvious. The influence of the evaporation rate is illustrated in Figure 8 for a PS/PVP sample of 50/50 composition, which has been dried in a saturated $CHCl_3$ atmosphere. Under these conditions no ordered structure is observable, only a few droplets with a broad size distribution are spreading on the surface. Accordingly, lowering the evaporation rate prevents the formation of an ordered pattern as it emerges at higher evaporation rates, as illustrated in Figure 5(a).

DISCUSSION

The processes occurring in a drying droplet of a ternary polymer solution of immiscible polymers are fairly complex and

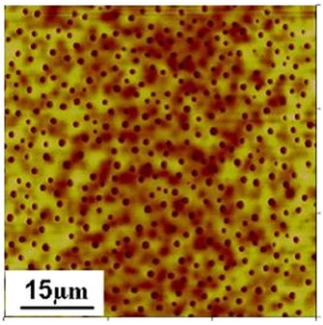

Figure 7. AFM topographical images of PS/PVP (90/10) blend film. [Color figure can be viewed in the online issue, which is available at wileyonlinelibrary.com.]

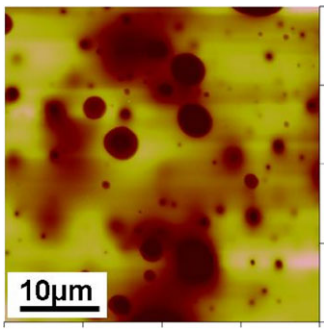

Figure 8. AFM topographical images of PS/PVP with the weight ratio of 50/50 prepared at a very low evaporation rate. [Color figure can be viewed in the online issue, which is available at wileyonlinelibrary.com.]

interdependent. Accordingly, we can consider the processes as an overlapping of three scenarios with increasing complexity. Taking a droplet of a volatile liquid as an example, convection of the capillary-, Marangoni- or Rayleigh type may occur, depending on the mechanical, dynamic, and thermal properties of the liquid.[11] Furthermore, there might be a type of capillary convection that causes an outward flow at the top layer of the drop provided by a contact pinning of the rim of the droplet.[26–29]

Substitution of the liquid with a binary solution, e.g. a polymer solution, exacerbates a simple solution to the drying drop problem. This is because the system becomes non-linear with increasing polymer content during the evaporation of the solvent. All the crucial properties of the solution undergo a continuous change and hence impede quantitative treatment. Finally, when adding a further polymer (the two polymers being immiscible) phase separation on reducing the solvent content of the blend solution additionally has to be taken into account. All these factors might play an important role in understanding the pattern formation at the surface of ternary polymer solutions.

In the following, we will focus on those compositions of our ternary polymer solution featuring an explicit surface pattern, e.g. the compositions from 60/40 to 30/70 PVP/PS weight fractions. As is obvious from Figure 6, surface structure formation has to be considered on the basis of phase separation pathways during evaporation because the bottom PVP layer is hardly explainable only by convective effects.

Phase Separation in the PS/PVP/$CHCl_3$ System

In order to gain some insight into the phase behavior of the PS/PVP/$CHCl_3$ system, a series of 50/50 PS/PVP solutions with increasing total polymer concentration from 3 to 17wt % were prepared and mixed carefully. For a total polymer concentration of 6wt % and higher, the solutions appeared turbid, indicating a two-phase liquid system. After quiescent storage of 24 h sedimentation induced separation of the phases which led to a layer of the individual phases [Figure 9(a)]. The majority of the initial solution separates into two phases. Additionally, for polymer concentrations above 6% a very thin, turbid layer is visible at the liquid-air interface, as has also been reported by Ohshima et al.[19] The two major precipitated phases were characterized by GPC in order to determine the PS/PVP ratio. In Figure 9(b) these compositional results from the GPC measurements are represented in a ternary diagram, showing that the solubility of PS in the PVP rich phase is markedly higher than vice versa. That means the bottom layer (PVP rich) contains a considerable amount of PS up to a certain total polymer concentration, whereas the PS rich phase appears to be more or less pure and without PVP content. Phase diagram of the PS/PVP/$CHCl_3$ system at room temperature determined from a 50/50 PS/PVP solution in $CHCl_3$ including the tie-lines. A series of different polymer concentrations was prepared and left for phase separation under quiescent conditions for 24 h. The solvent content of each precipitated phase was measured gravimetrically; the polymer composition was determined by GPC.

Convective Transport to the Droplet Rim

For a drying droplet the coffee-stain effect is well understood and based on the pinning of the substrate-liquid-air line in combination with the capillary convection-driven transport of solution from the center to the rim of the droplet.[26] However, the ternary PS-PVP-$CHCl_3$ system we investigated cannot be treated as an ideal solution and one has to take other effects into consideration as well. Evaporation of the solvent will induce thermal, viscosity, and concentration gradients in the droplet which finally lead to convective flows having an inward component as well. One has to assume that this inward directed flow is located close to the substrate since on the surface of the

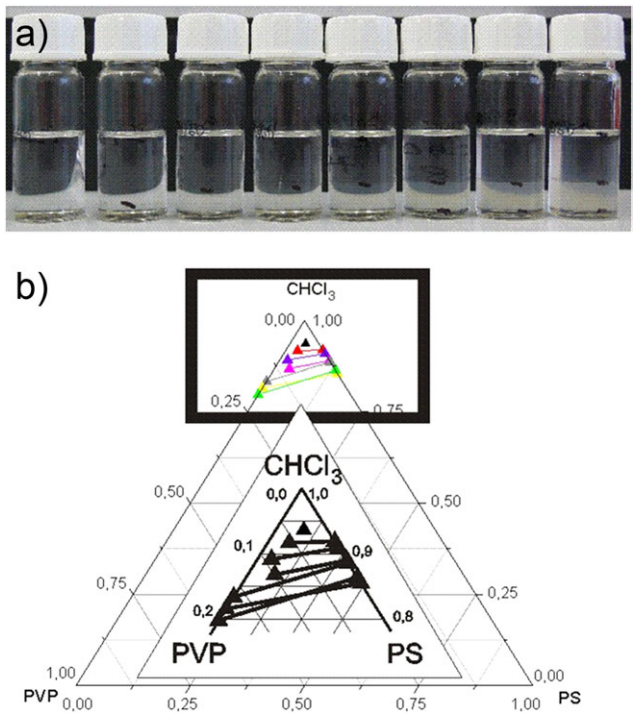

Figure 9. Phase diagram of the PS/PVP/$CHCl_3$ system at room temperature determined from a 50/50 PS/PVP solution in $CHCl_3$ including the tie-lines. A series of different polymer concentrations was prepared and left for phase separation under quiescent conditions for 24 h. The solvent content of each precipitated phase was measured gravimetrically; the polymer composition was determined by GPC. [Color figure can be viewed in the online issue, which is available at wileyonlinelibrary.com.]

Applied Polymer SCIENCE

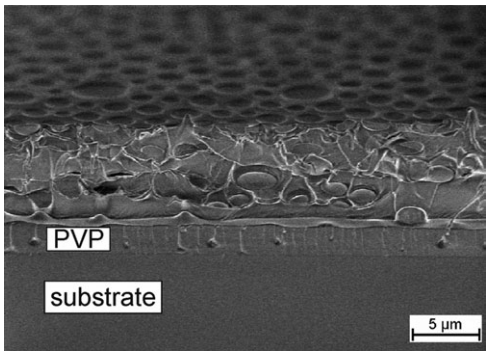

Figure 10. SEM micrograph showing a cross section of a thick area of a 50/50 PS/PVP dried film, illustrating the sedimentation of PVP rich domains from the solution-air interface.

droplet the outward flow appears. The inward transport process balances the excess solution arriving at the droplet rim, otherwise the droplet would quickly become a ring-like shape with all the solution accumulated along the pinned rim. Since this is not the case, there has to be an additional flow close to the substrate back to the centre of the droplet. Accordingly, for a drying droplet there is a convective cycle running outward at the air-solution interface and returning inward at the substrate-solution interface.

Additionally, the local concentration (or the evaporation rate) is higher at the rim area; which is actually the driving force for the convection mechanism. Conversely, it can be argued that the phase separation should appear first at the rim of the droplet. Moreover, the solidification of the polymer-solvent system will start at the rim as well, propagating into the central area of the droplet.

Pattern Formation

From the above we now can assume a plausible route for the pattern formation of a drying droplet of a binary PS/PVP polymer solution. Directly after applying the solution to the substrate, the capillary-driven convective flow toward the rim of the droplet sets in together with a substrate-near, backward flow of the solution. Concurrently, evaporation of the solvent continuously increases the total, as well as the local polymer concentration at the air-solution interface. Hence, the higher concentrated polymer solution is transported to the rim, accompanied by a higher evaporation rate that is present there. Accordingly, the first phase separation process will take place at the rim of the droplet. The dense PVP rich phase will slump to the substrate and is captured by the substrate near inward flow, resulting in a re-dissolution of this phase. The less dense PS rich phase on the surface of the droplet will, at this stage, accumulate at the rim as is evident in Figures 3 and 4.

With the proceeding solvent evaporation the average polymer concentration increases. This in turn is accompanied by an increase in the overall viscosity of the droplet solution and, more important, by decreasing dynamics. Finally, the local polymer concentration at the air-liquid interface of the droplet will exceed the miscibility limit. Liquid–liquid phase separation sets in via a nucleation and growth process of a PVP rich domain in a PS rich matrix and PVP droplets nucleate and grow at the air-liquid interface. As long as the current viscosity allows, these PVP domains will sink down to the substrate surface and form a PVP rich layer as can be observed in the SEM micrograph of Figure 6. An even more expressive snapshot of this domain sedimentation is shown in Figure 10, where the PVP rich domains are captured on their way down to the substrate.

SEM micrograph showing a cross section of a thick area of a 50/50 PS/PVP dried film, illustrating the sedimentation of PVP rich domains from the solution-air interface.

As long as the PVP domains can sink down to the substrate, the global, convective flow towards the droplet rim is present as well. Hence, the remaining PVP domains will be pushed together by the surface near flow yielding some kind of closely packed structure. Furthermore, close inspection of the Fourier-transform of the surface pattern [insets in Figure 5(a,b)] reveals a slightly elliptical shape which is an indication of this unidirectional deformation. When finally the increasing viscosity of the system disables any further movement, this surface structure is vitrified, as found in Figures 3(b) and 5(a,b). Accordingly, the observed surface pattern is a snapshot of a liquid–liquid phase separation including the following growth process. The alignment of the PVP domains is thought to be only the result of a closely packing mechanism induced by the typical, surface-near outward convection observed for a drying droplet and not, as speculated for other systems,[8–10,14,15] the effect of Marangoni convection.

This relationship is illustrated schematically in Figure 11, showing an idealized phase separation bimodal for a three component system. During the evaporation of the solvent, the system transverses along the dotted line toward the base line. For

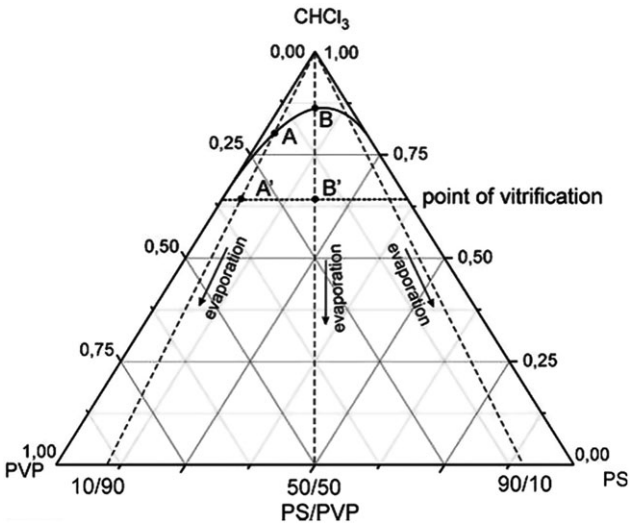

Figure 11. Schematic phase diagram for demonstration of the inter-relationship between the "evolution time" and the initial polymer composition. The system traverses along the evaporation lines through the phase diagram. The point of vitrification is denoted as a horizontal line (at an arbitrary solvent concentration). The structure formation takes place between intersection of the phase spinodal (Point A or B) and the point of vitrification (Point A′ or B′).

reasons of simplicity we neglected any tie-lines and just considered the entire, momentary composition of the system. Assuming, that the (mean) viscosity of the system depends only on the solvent fraction and, as a first order approximation, independents on the PS/PVP ratio, the "point of vitrification" corresponds to a horizontal line in the phase diagram. Accordingly, during evaporation the system traversed along the evaporation line and intersected the binodal at point A or B, dependent on the initial PS/PVP ratio. At this point, phase separation and the following structure formation processes set in until the system intersected the "point of vitrification" at which all structure evolution stopped. The "evolution time", e.g. the time for the system to traverse from point A to A′, depends on the ratio of the two polymers (and on the specific shape of the binodal line). Typically, the evolution time is highest for a balanced ratio of the two polymer components (as denoted in Figure 11 by points B and B′) and decreases for high ratios of major-to-minor compositions. The schematic phase diagram demonstrates the inter-relationship between the "evolution time" and the initial polymer composition. The system traverses along the evaporation lines through the phase diagram. The point of vitrification is denoted as a horizontal line (at an arbitrary solvent concentration). The structure formation takes place between intersection of the phase spinodal (Point A or B) and the point of vitrification (Point A' or B').

Given the above, the observed surface patterns can be interpreted in terms of a dynamic process comprising nucleation and growth of phase domains, coalescence, and sedimentation. For the 10/90 PS/PVP blend the "evolution time" is very short and hence the pattern, consisting of some irregular, protruding spots, is a snapshot of the early stage of domain growth of a PS rich phase in a PVP matrix [Figure 1(a,c)]. The difference to the surface of the 20/80 PS/PVP film is evident, the PS rich domains grew bigger to a bimodal distribution as shown in Figure 1(b,d). Taking into consideration that (a) the nucleation density is higher and (b) the "evolution time" is longer in the latter case, the pattern shown in Figure 1(b) is a result of a longer domain growth period in combination with subsequent coalescence of the PS rich droplets. Similarly, the structure formation for compositions with PVP as the minor component can be considered. Due to the short "evolution time" the observed surface pattern in Figure 7 can be interpreted as a snapshot of the early stage of nucleation and growth of PVP domains. It is worth noting that the size of the domains is quite uniform [as compared to Figure 1(a)], which is an indication of a much shorter induction time for the nucleation of PVP rich domains.

When increasing the evaporation time to around 8 minutes, as in the preparation of Figure 8, the respective "evolution time" will increase, giving the system more time within the dynamic viscosity window to reach thermodynamic equilibrium. Accordingly, the surface pattern presented in Figure 8 is dominated by a combination of coalescence and sedimentation effects.

CONCLUSIONS

The formation of an ordered surface pattern in a PS/PVP binary polymer solution is a delicate interplay of the liquid–liquid phase separation with subsequent domain growth and the increase of the overall viscosity of the system. This just vitrifies all the structures present at a certain point of time, or specifically at a certain total polymer concentration. For a high evaporation rate, this vitrification point is reached quite fast with the effect that the phase separation-induced morphology is not well developed. Accordingly, we observed an irregular surface pattern with only a few domains, differing in size. For very low evaporation rates the point of "freezing" is retarded and hence the morphology at the end of the phase separation process is fixed, e.g. the effect of the sedimentation process on the appearance of the domain-distribution becomes dominant.

In other words, the solvent evaporation induces two processes: first, the liquid–liquid phase separation, being a dynamic process involving nucleation, domain growth; second, sedimentation of the denser phase. Simultaneously, the solvent evaporation also induces a structure fixation via increasing viscosity. Hence, the evaporation rate can be considered as a time-lag for capturing a certain snapshot of the phase separation morphology.

ACKNOWLEDGMENTS

The authors would like to thank Christine Rosenauer and Ute Heinz for GPC measurements and Gunnar Glasser for SEM examination. Moreover, Xiaoli Sun would like to acknowledge the financial support she received from the International Max Planck Research School (IMPRS) and National Natural Science Foundations of China (No. 21004003, 21174014). Furthermore, the authors would like to acknowledge the fruitful discussions with Prof. G. Wegner.

REFERENCES

1. Yabu, H.; Shimomura, M. *Adv. Funct. Mater.* **2005**, *15*, 575.
2. Hiller, J.; Mendelsohn, J. D.; Rubner, M. F. *Nat. Mater.* **2002**, *1*, 59.
3. Tanev, P. T.; Chibwe, M.; Pinnavaia, T. J. *Nature* **1994**, *368*, 321.
4. Li, F.; Wang, Z. Y.; Ergang, N. S.; Fyfe, C. A.; Stein, A. *Langmuir* **2007**, *23*, 3996.
5. Yang, S.; Horibe, Y., Chen, C. H.; Mirau, P.; Tatry, T.; Evans, P.; Grazul, J.; Dufresne, E. M. *Chem. Mater.* **2002**, *14*, 5173.
6. Cheng, C. X.; Tian, Y.; Shi, Y. Q.; Tang, R. P.; Xi, F. *Macromol. Rapid Commun.* **2005**, *26*, 1266.
7. Muller-Buschbaum, P.; Gutmann, J. S.; Stamm, M. *Macromolecules* **2000**, *33*, 4886.
8. Wang, Y.; Liu, Z. M.; Han, B. X.; Gao, H. X.; Zhang, J. L.; Kuang, X. *Chem. Commun.* **2004**, 800.
9. Wang, Y.; Liu, Z. M.; Huang, Y.; Han, B. X.; Yang, G. Y. *Langmuir* **2006**, *22*, 1928.
10. Cui, L.; Han, Y. C. *Langmuir* **2005**, *21*, 11085.
11. Probstein, R. F. Physicochemical Hydrodynamics; Butterworths: Boston, **1989**, p 353.
12. Zhang, J.; Beringer, R. P. *Phys. Rev. E* **2007**, *76*, 016306.
13. Pearson, J. R. A. *J. Fluid Mech.* **1958**, *4*, 489.

14. Kumacheva, E.; Li, L.; Winnik, M. A.; Shinozaki, D. M.; Cheng, P. C. *Langmuir* **1997**, *13*, 2483.
15. Mitov, Z.; Kumacheva, E. *Phys. Rev. Lett.* **1998**, *81*, 3427.
16. Cui, L.; Wang, H.; Ding Y.; Han, Y. *Polymer* **2004**, *45*, 8139.
17. Wu, K. H.; Lu, S. Y.; Chen, H. L.; Chen, Y. Y. *Macromol. Chem. Phys.* **2008**, *209*, 615.
18. Wu, K. H.; Lu, S. Y.; Chen, H. L. *Langmuir* **2006**, *22*, 8029.
19. Kim, J. K.; Taki, K.; Ohshima, M. *Langmuir* **2007**, *23*, 12397.
20. Bormashenko, E.; Whyman, G.; Pogreb, R.; Stanevsky, O.; Hakham-Ithhaq, M.; Gendelman, O. *Israel J. Chem.* **2007**, *47*, 319.
21. de Gennes, P. G. *Eur. Phys. J. E* **2001**, *6*, 421.
22. Wiltzius, P.; Cumming, A. *Phys. Rev. Lett.* **1991**, *66*, 3000.
23. Cumming, A.; Wiltzius, P.; Bates, F. S.; Rosedale, J. H. *Phys. Rev. A* **1992**, *45*, 885.
24. Cumming, A.; Wiltzius, P.; Bates, F. S. *Phys. Rev. Lett.* **1990**, *65*, 863.
25. Shi, B. Q.; Harrison, C.; Cumming, A. *Phys. Rev. Lett.* **1993**, *70*, 206.
26. Deegan, R. D.; Bakajin, O.; Dupont, T. F.; Huber, G.; Nagel, S. R.; Witten, T. A. *Nature* **1997**, *389*, 827.
27. Deegan, R. D. *Phys. Rev. E*, **2000**, *61*, 475.
28. Deegan, R. D.; Bakajin, O.; Dupont, T. F.; Huber, G.; Nagel, S. R.; Witten, T. A. *Phys. Rev. E* **2000**, *62*, 756.
29. Xu, J.; Xia, J. F.; Hong, S. W.; Lin, Z. Q.; Qiu, F.; Yang, Y. L., *Phys. Rev. Lett.* **2006**, *96*, 066104.